Application of *In Situ* Neutron Diffraction to Characterize Transient Material Behavior in Welding

ZHENZHEN YU,[1] ZHILI FENG,[1,3] WAN CHUCK WOO,[2] and STAN DAVID[1]

1.—Materials Science and Technology Division, Oak Ridge National Laboratory, Oak Ridge, TN 37831, USA. 2.—Neutron Science Division, Korea Atomic Research Institute, Daejeon 305 353, South Korea. 3.—e-mail: fengz@ornl.gov

A fundamental understanding of the transient and nonequilibrium material behavior during welding is essential in the pursuit of process control and optimization to produce defect-free, structurally sound, and reliable welds. The deep penetration capability of neutrons into most metallic materials makes neutron diffraction a unique and powerful tool in understanding the material structures and properties. However, the inadequate neutron flux limits its application in time-resolved study of transient material behavior. This article highlights recent developments toward *in situ* time-resolved neutron diffraction measurement of material behavior during welding with two examples: (I) measurement of the transient temperature and thermal stresses during friction-stir welding of an aluminum alloy and (II) measurement of the solid-state phase transformation behavior of an advanced high-strength steel under thermal conditions comparable to the welding processes. These newly developed experimental approaches can be broadly applied to other welding or thermomechanical processes for time-resolved measurement of the fast-changing material state in structural metals.

INTRODUCTION

As an important modern manufacturing technology, welding is widely used in the construction of buildings and bridges, and in ship building, aerospace, automotive, chemical, petroleum, and electric and power generation industries. Over the years, welding has evolved into a major interdisciplinary technology field requiring synthesis of knowledge from various disciplines.[1]

Many widely used welding processes, including arc, laser, and electron-beam, to name a few, use a localized heating source to join materials together. These processes are characterized by a highly transient and nonuniform temperature field, rapid heating and cooling, and nonequilibrium phase transformations, which can greatly influence the final microstructure, properties, and performance of a welded structure. For instance, advanced high-performance structural metals and alloys, such as high-strength steels, Al alloys, and nickel-based super alloys, require carefully designed and controlled thermomechanical processing to achieve the desired microstructure and superior properties. However, a welding operation can alter their microstructure, resulting in considerable property degradation.[2–8] As an example, Fig. 1 depicts the phenomenon of heat-affected zone (HAZ) softening in an advanced high-strength steel (AHSS) weld for automotive applications. In this particular case, excessive HAZ softening leads to premature failure in the HAZ and a reduced joint strength. The HAZ softening is a product of the nonequilibrium phase transformation, and its extent strongly depends on the steel chemistry and the welding thermal history.[8] Solutions to effectively control and minimize the HAZ softening and strength reduction rely on fundamental understanding of the mechanisms and quantitative description of the kinetics of nonequilibrium phase transformation processes in this class of steels having a wide chemical composition range and under 10^1–10^3°C/s heating/cooling rates typically associated with welding.

The localized heating and nonuniform cooling during welding also leads to the development of stresses, which are locked up as residual stresses in
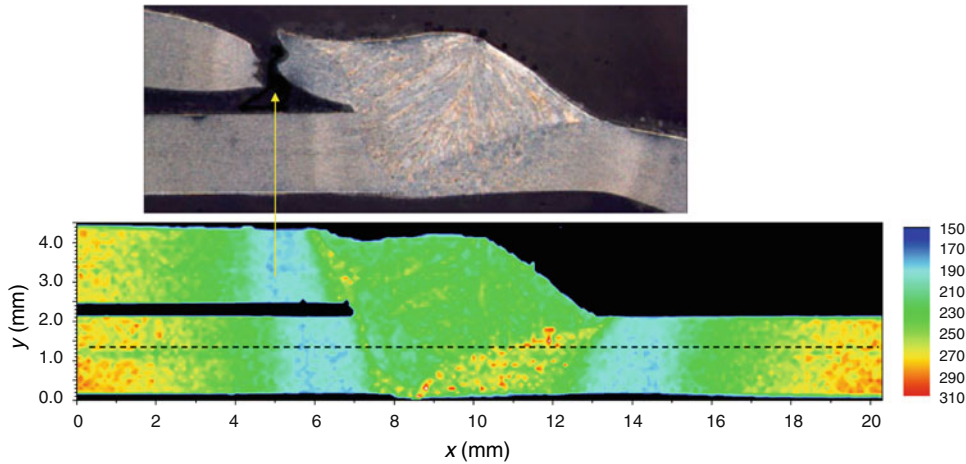
Fig. 1. Vickers microhardness distribution in a DP980 advanced high-strength steel weld made by gas-metal arc welding. The failure location under tensile loading corresponds to the HAZ softening region.

the weldments after cooling down. High tensile residual stresses typically present in the weld region are detrimental to the performance and the structural integrity of the welded components, e.g., reducing their fatigue life.[9,10] Solid-state phase transformations during welding of alloys may also affect the stress development by the localized volume expansion/contraction associated with phase changes.[9,11–13] For example, the principle of low temperature martensitic phase transformations has been utilized in developing a special class of ferritic welding consumables for effectively reducing the tensile residual stresses in the weldments.[14] Similar phenomena can occur in solid-state joining processes as well. For instance, Yu et al.[15] reported that during friction-stir welding (FSW) of Mg alloy AZ31B, the heating rate peaked at ∼15°C/s, and the strain rate was between 0.5 s^{-1} and 250 s^{-1}. Such severe thermomechanical parameters in the weldments interplay with each other and determine the evolution of new microstructure (e.g., phases, grain size, and texture), the development of stresses, and the resulting material properties.[16–20]

It is well recognized that quantitative understanding of the transient and nonequilibrium material behavior plays a critical role in the pursuit of process control and optimization to produce defect-free, structurally sound, and reliable welds. However, to date, such information is limited due to challenges in direct nondestructive measurement of the transient material states under the complex thermomechanical conditions of welding. Conventional postmortem weld characterizations using optical and electron microscopy, atom probe field ion microscopy, laboratory x-ray, and other experimental techniques have only yielded rudimentary understanding on the *evolution* of microstructure and stresses *during* a welding operation.

Synchrotron x-ray diffraction and neutron diffraction techniques, with the increase in flux and the advancement in detectors and instruments over

the past two decades, have become powerful tools to study the material's behavior including residual stress,[21,22] temperature and stresses development,[10,23–28] thermal expansion,[29,30] phase transformation,[12,31–35] and texture evolution[18,36,37] associated with various thermomechanical manufacturing processes. Although similar in many aspects, synchrotron x-ray and neutron diffraction have two important differences when applied to study the fast transient material behavior related to welding: the penetration depth and the time resolution of a measurement.

The relatively low penetration (up to several millimeters) limits synchrotron x-ray diffraction to thin sample or near surface measurements.[10,24,38] Neutrons have an effective penetration depth on the order of centimeters, which enables nondestructive, bulk-volume-averaged *in situ* study[39,40] of the large structure/components in complex sample environments. Synchrotron x-rays are most suitable for two-dimensional stress measurements. The strain/stress along the out-of-plane direction cannot be detected since the short wavelength (high energy) of synchrotrons results in Bragg diffraction only at small angles.[10,38] In comparison, neutrons can examine the stresses along three principal directions in the welds of bulk components with spatial resolution of as small as 1 mm.[10,38]

Synchrotron x-ray diffraction has relatively good time resolution. For example, a time resolution on the order of second can be readily achieved for phase transformation measurement during gas tungsten arc spot welding of carbon steels.[41] On the other hand, the relatively low flux is a major limitation for time-resolved neutron diffraction experiment. Even with today's most powerful neutron source, it is extremely challenging to achieve time resolution of 1 s or less with a sample volume of 1 mm^3 for most engineering materials such as steels and Al alloys.[28,42] Such a drawback in temporal resolution limited the application of neutron diffraction to

investigate fast thermomechanical processes in real time.

This article highlights two recent developments on experimental approaches to overcome the temporal resolution limit of neutron diffraction, so that the deep penetration capability of neutrons essential to probe inside a material can be effectively utilized for *in situ* time-resolved measurement of material behavior under fast transient welding conditions: (I) *in situ* time-resolved measurement of the transient temperature and thermal stresses during FSW of an aluminum alloy and (II) *in situ* time-resolved measurement of the solid-state phase transformation kinetics of an AHSS under thermal conditions comparable to the welding processes. These experimental approaches can be broadly applied to other welding or thermomechanical processes for time-resolved measurement of the fast-changing material state in structural metals.

IN SITU MEASUREMENT OF TEMPERATURE AND STRESS

FSW is a novel and revolutionary solid-state joining process invented in the 1990s.[43] Fundamentally, FSW relies on extensive thermomechanical deformation to create metallurgical bonding and join materials together. Temperature and stress distributions generated by the process determine the success of the welding operation. More importantly, the thermomechanical history is essential for the microstructure evolution in the processing zone, which directly affects the final material properties.[16–20]

Woo et al.[27,28,42] developed a methodology to directly measure the temperature and stress simultaneously during FSW of 6061-T6 Al alloy using *in situ* time-resolved neutron diffraction. The *in situ* neutron diffraction measurement was performed at the Spectrometer for MAterials Research at Temperature and Stress (SMARTS) of Los Alamos Neutron Science Center. A remotely operated, portable FSW machine was purposely built, and the experiment setup is shown in Fig. 2. Commercial 6061-T6 Al plate measuring 965 mm long, 178 mm wide, and 6.35 mm thick was used. The welding speed was 0.42 mm/s, and the tool rotation speed was 156 rev/min. The diameters of the tool shoulder and threaded pin were 25.4 mm and 6.35 mm, respectively. The neutron scattering volume was $3 \times 2 \times 2$ mm^3.

To overcome the low neutron flux, a limiting factor for directly measuring the fast transient material state, Woo et al.[42] developed a novel method to increase the time resolution of neutron diffraction experiment based on two principles: (I) the existence of the quasi-steady state (QSS) in many thermomechanical processes and (II) the material states under QSS is stationary to the detector that is fixed in space relative to the welding arc (the so-called *Eulerian* observer). During welding, the
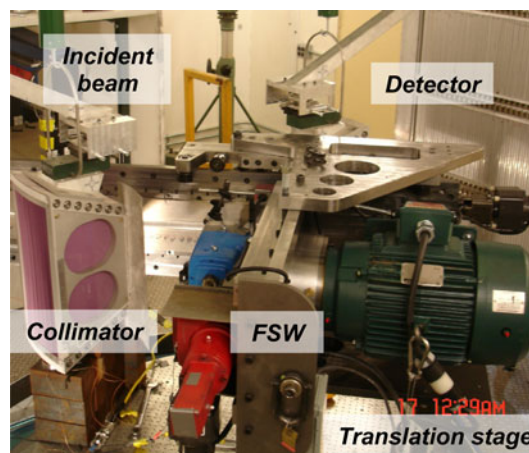

Fig. 2. A portable FSW machine was installed at SMARTS facility for *in-situ* neutron measurement.

temperature field in the workpiece is governed by the net energy balance between the heat generation by the welding heat source and the heat dissipation through the workpiece and the surrounding materials. When the heat input balances the heat diffused away, the temperature field in the workpiece reaches the QSS, which is stationary (independent of time) relative to an observer who travels with the welding heat source. Measurement in the Eulerian reference system under QSS makes it possible to allow for sufficient time to collect the diffracted neutrons under the same temperature, stress, and material state conditions. Special experiment setup and testing procedures were implemented for the *in situ* time-resolved FSW measurement, as illustrated in Fig. 3. In the experiment, the welding head was fixed in space at a predetermined position relative to incident neutron beam, and the workpiece was instead to travel along the longitudinal direction to achieve the QSS condition and to allow for the measurement in *Eulerian* reference frame.

To experimentally confirm the existence of QSS in FSW, *d* spacing changes of Al (311) were measured by keeping neutron source at a fixed constant distance away from the tool center. Figure 4 shows the *d* spacing change in the transverse direction during the FSW measured at 15 mm away from the tool center. A temporal resolution of 2 min was obtained in the neutron diffraction measurement. For the first 3 min after the tool was plunged into the Al plate, the *d* spacing increased drastically, associated with the initial transient stage in which the temperature begins to build up and the stress field to develop. After the initial transient stage, *d* spacing remained relatively constant with relatively small variations (within the neutron scattering uncertainty range as indicated by the error bar in the figure) for about 18 min, indicating that an 18-m in QSS was achieved, which is far more than adequate to obtain sufficient diffracted neutrons for *d*-spacing measurement. After completion of the FSW process,
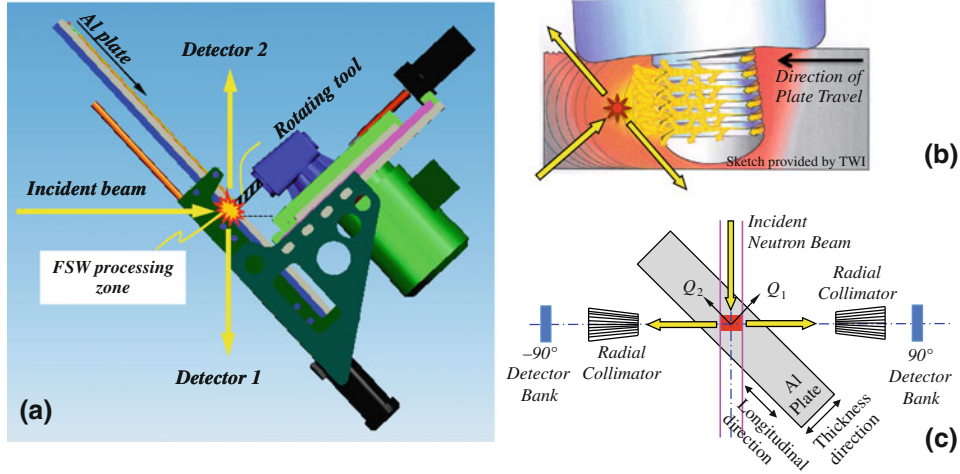
Fig. 3. Schematics illustrate the key features in *in-situ* neutron diffraction measurement of FSW process in the Eulerian reference frame under the QSS conditions: (a) the welding head is fixed in space relative to the stationary neutron beam whereas the Al plate (the workpiece) moves towards the neutron beam; (b) the measurement location inside the workpiece and underneath the FSW tool; and (c) neutron beam arrangement for the simultaneous measurement of the longitudinal and the normal strain components.
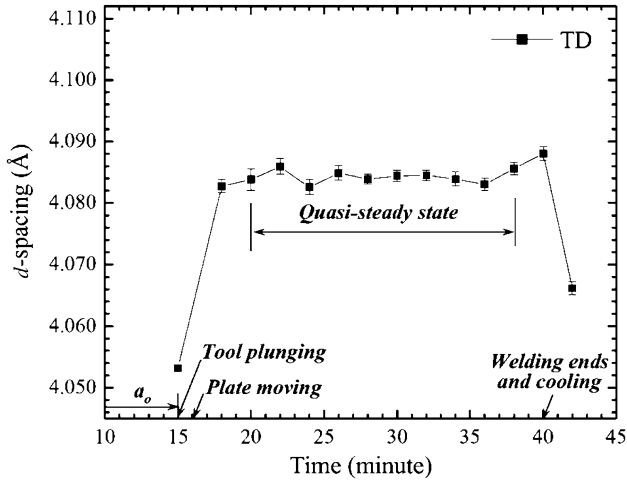

Fig. 4. Evolution of *d* spacing in transverse direction during FSW by neutron diffraction measurement at 15 mm behind the welding tool (Copyright © Maney Publishing) (after Woo et al.[28]).

the plate began to cool down and the *d* spacing corresponded with a significant drop. Confirmation of the existence of the QSS condition enables the study of the transient behavior with a series of QSS measurements of *d* spacing changes along three orthogonal (longitudinal, transverse, and normal) directions.

The *total* lattice strain is calculated from the lattice spacing change measured by neutron diffraction. It consists of the elastic strain due to stress, thermal stress due to temperature change, and the expansion/contraction from phase transformation. The total lattice strain can be expressed by

$$\varepsilon = \frac{d - d_0}{d_0} \tag{1}$$

where d is the d spacing under the stress and temperature during welding, and d_0 is the reference stress-free d spacing before the start of welding.

The FSW plate was considered as a macroscopically isotropic polycrystalline material subject to a time-dependent thermoelastoplastic deformation process. The material is initially stress free at room temperature. The transient stress during the thermomechanical process can be estimated with Eq. 2.

$$\sigma_i = \frac{E}{1+v}\left(\varepsilon_i - \varepsilon_z\right) + \sigma_z = \frac{E}{1+v}\frac{d_i - d_z}{d_0} + \sigma_z$$

$$= \frac{E}{1+v}\frac{d_i - d_z}{d_z} + \sigma_z \quad (i = x, y) \tag{2}$$

where σ, E, and v are the transient stress, elastic modulus, and Poisson's ratio. The authors substituted d_0 in Eq. 2 by d_z for the determination of stress. d spacing of the stress free sample was measured to be ~4.05 Å and the maximum d spacing during the welding was measured to be ~4.085 Å. Hence, the maximum error in stress calculation induced by the substitution of d_0 was estimated to be less than 0.9%. The reason for the substitution of d_0 is that in many engineering situations, the microstructure inhomogeneity and/or internal built-in stresses precludes the possibility of measuring d_0. Eliminating the need to know d_0 makes the *in situ* neutron diffraction measurement of time-resolved stress changes in thermoelastoplastic deformation processes a realistic approach.

The temperature was also calculated from the strain components as expressed in Eq. 3.

$$T = T_0 + \frac{1}{\alpha}\left[\frac{v}{1+v}\left(\varepsilon_x + \varepsilon_y\right) + \frac{1-v}{1+v}\varepsilon_z\right] - \frac{1-2v}{\alpha E}\sigma_Z \tag{3}$$

where T and α are the temperature and thermal expansion coefficient. It is noted that the coefficient of thermal expansion often takes in consideration of phase transformation also. A thermocouple was attached on the backside of the plate near the scattering volume. The good agreement between the temperature profiles recorded by thermocouple and obtained from neutron scattering verified the validation of such method.

The QSS data can be input into Eqs. 2 and 3 to calculate the transient stress and temperature as a function of distance from the tool. Note that outside of the rotating tool, the stress state was considered as plane stress, i.e., $\sigma_z = 0$ in Eq. 2. Underneath the tool shoulder, the normal stress σ_z was calculated from the forging force of the FSW process and the tool diameter, which was estimated to be -17 MPa. According to Eq. 3, a stress value of -17 MPa would cause a temperature change of about 5°C. At elevated temperatures, the material softens and the flow stress decreases. Since the stresses in the stir zone are bounded with the flow stresses, the uncertainties in temperature due to the lack of accurate σ_z information should be relatively small. For instance, the temperature difference should be less than 15°C corresponding to a flow stress of 50 MPa at elevated temperature of 322°C. Note that the calculation of stress and temperature in Eqs. 2 and 3 used temperature dependent elastic modulus of Al6061.

With this methodology, the *in situ* neutron diffraction measurement, for the first time, revealed the temperature and stress changes as a function of time in the stir zone of Al6061-T6 alloy weld. The maximum temperature was observed underneath the tool, reaching 362°C. As shown in Fig. 5, compressive thermal stresses developed in the vicinity of the rotating tool, with the higher compressive stress in the longitudinal direction (σ_x). As the weld metal cools down from the stirring region, the stresses changed to tension, and higher tension stresses developed along the longitudinal direction.

TRANSIENT PHASE TRANSFORMATION BEHAVIOR MEASUREMENT

Phase transformation is commonly associated with welding and other thermomechanical manufacturing processing. AHSS are an integral part of the materials solution for automotive industry to produce highly crash-resistant body structures while reducing the vehicle weight for fuel efficiency. However, welding and other manufacturing processes usually lead to unexpected property degradation of the final fabricated AHSS components[3,6,8,44,45] due to nonequilibrium phase transformation under fast-changing thermomechanical process conditions. Our knowledge of nonequilibrium phase transformation is very limited in such complex alloy system during fast heating and cooling conditions, largely due to the lack of direct experimental measurement techniques to identify and quantify the transient transformation process.

Yu et al.[35] developed a neutron diffraction experimental approach for direct *in situ* measurement of nonequilibrium phase transformations of AHSS with a subsecond time resolution under fast heating/cooling conditions comparable to those during arc welding processes. One material used in this study was a dual-phase AHSS, DP980, with nominal chemical composition of Fe-0.15%C-1.32%Mn-0.32%Si-0.04%Al-0.03%Cr-0.02%Cu-0.01%Ni (all in wt%). The steel sheet has a thickness of 2 mm. An electrical resistance-heating device was designed and built to enable controlled heating rates during *in situ* neutron diffraction measurements, as shown in Fig. 6. In order to study the nonequilibrium phase transformation kinetics
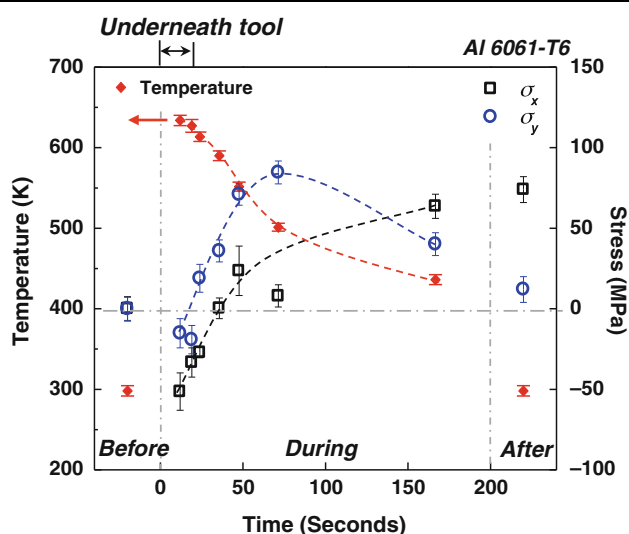

Fig. 5. Transient stress and temperature distributions along weld centerline as a function of time before, during, and after friction-stir welding process. σ_x and σ_y are the stresses along longitudinal and transverse directions.
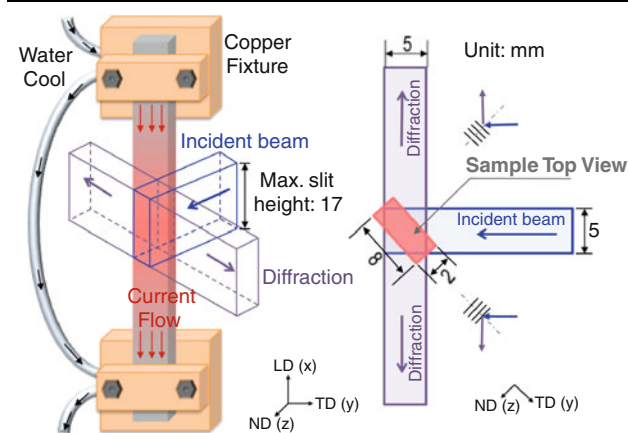

Fig. 6. Schematic drawing of experimental setup for *in situ* neutron diffraction measurement of phase transformation kinetics. LD, ND, and TD denote longitudinal direction, normal direction, and transverse direction, respectively.

at different heating rates, the samples were heated up to 1050°C in an Argon gas atmosphere to prevent oxidization of samples, under controlled rates of 3°C/s and 30°C/s, respectively, and then allowed to cool naturally to room temperature.

Time-of-flight neutron diffraction measurement of the phase transformation process was performed at the engineering diffractometer, VULCAN beam line at the Spallation Neutron Source (SNS)[46] at Oak Ridge National Laboratory. A spallation neutron source is an accelerator-driven, pulsed neutron source, where neutrons are generated by spallation rather than nuclear fission as in a reactor-based neutron source. VULCAN beam line at the SNS has a neutron flux of 6.7×10^7 neutrons cm^{-2} s^{-1} pulsed at 60 Hz on the sample.

The neutron data and temperature data were collected continuously while sample was subject to heating and cooling. For the pulsed neutron beam, the full peak pattern diffracted from the multiple crystallographic lattice planes in a particular material direction is usually analyzed by the Rietveld refinement method[47–49] with GSAS software (NIST, Gaithersburg, MD),[50,51] which makes use of the entire diffraction pattern by fitting all the diffraction peaks to a structural model of the material. The precision of lattice parameter calculation ($\Delta a/a$) by Rietveld refinement method is approximately $0.5–1 \times 10^{-4}$, corresponding to a temperature increment of about 3–6°C based on the thermal expansion equation of ferrite phase in DP980.[35] Hence, a target temperature resolution of 3°C was chosen for the *in situ* heating measurement at both the slow and fast heating rates. In other words, for the 30°C/s heating rate case, about 0.1 s temporal resolution is required for a temperature resolution of 3°C. Such subsecond temporal resolution requirement was achieved through (I) optimizing special sample configurations that maximize the diffraction volume to increase the intensity of diffraction pattern, and at the same time, minimize the temperature gradient within the diffraction volume to maintain measurement accuracy; and (II) applying the stroboscopic technique[52,53] to further enhance the diffraction intensity.

At VULCAN beam line, the gauge volume is defined by the incident slits, the receiving collimators, and the sample thickness. The maximum attainable gauge volume is $8 \times 17 \times 2$ mm^3 for the measurement, as illustrated in Fig. 6. This maximum neutron gauge volume was used to increase neutron counts. To obtain a relatively uniform temperature distribution within the diffraction volume, the specimen's geometry and dimensions were optimized by means of transient electrical-thermal finite-element modeling. The optimized sample dimensions were 8 mm in width and 240 mm in length. For a slow-heating case (3°C/s), notches were made near the ends of the sample to increase the local heat generation while restricting heat loss to the fixtures. Additionally, the temperature
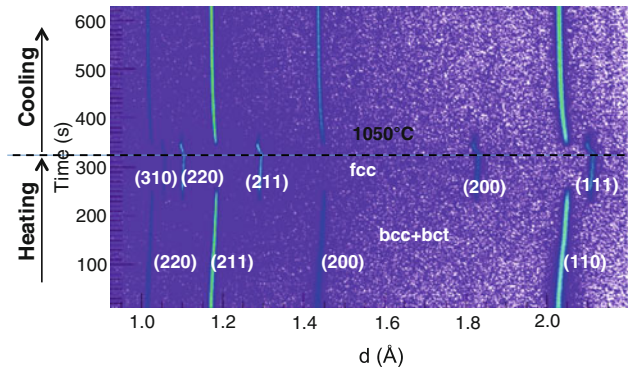

Fig. 7. At a heating rate of 3°C/s, neutron diffraction pattern evolution as a function of time in DP980 reveals the phase transformation process (bcc = body-centered cubic; bct = body-centered tetragonal; fcc = face-centered cubic).

uniformity was experimentally verified with thermocouples attached on the sample surface to record the temperature distribution, which showed that a temperature gradient less than 3°C within the diffraction volume was achieved. With the relatively strong neutron flux at VULCAN beam line and such experimental setup, for the first time, direct *in situ* measurement of the phase transformation behavior in AHSS achieved a time resolution of 1 s. A 3°C temperature resolution was obtained for experiments with 3°C/s heating rate. Figure 7 shows the evolution of diffraction patterns in DP980 as a function of temperature with a heating rate of 3°C/s. Note that peak pattern of martensite (body-centered tetragonal, α_M) phase cannot be distinguished from that of ferrite (body-centered cubic, α) since the lattice parameters of α and α_M are fairly close.[54]

The intensity of neutron diffraction peaks in unit time was further enhanced utilizing a stroboscopic technique in order to achieve the subsecond resolution for faster heating conditions. Such a technique allows the superimposition of diffraction patterns at given temperature values from different heating–cooling cycles. For instance, in the measurement of phase transformation at 30°C/s, ten thermal cycles (heating and cooling) were repeated, and only cycles with temperature deviations less than 3°C were selected for peak pattern superimposition.

Figure 8 shows an example of on-heating phase transformation behavior from ferrite (α) + martensite (α_M) to austenite (γ) in DP980 at the two different heating rates. The effects of heating rate on the kinetics of phase transformation, represented by the variations of volume fractions as a function of temperature, were clearly revealed and quantified. For example, as the heating rate increases, both the initiation and completion of the phase transformation process were shifted to higher temperature level. More interestingly, the *in situ* neutron diffraction measurement revealed that there is a drastic change in the phase transformation kinetics as the heating rate increases. At 3°C/s, a two-stage
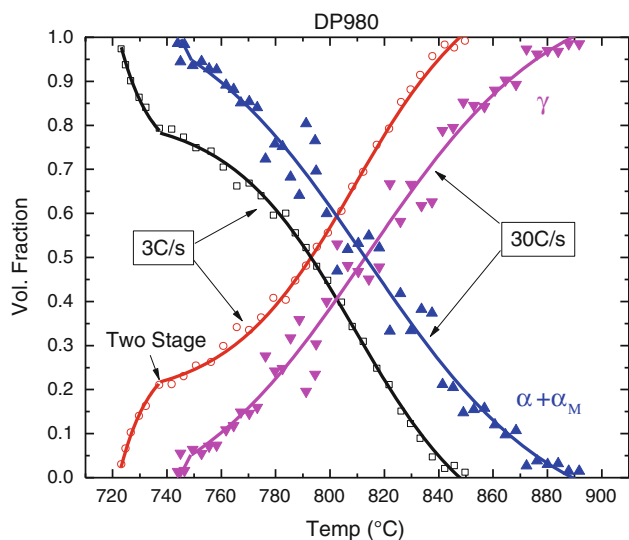
Fig. 8. Phase transformation from ferrite (α) + martensite (α_M) to austenite (γ) in DP980: variations of their volume fractions as a function of temperature.

phase transformation process was observed. At the earlier transformation stage, the formation rate of austenite was much faster, possibly due to the presence of carbon-rich site for austenite to nucleate first.[33] Such two-stage phase transformation was not as apparent in the higher heating rate (30°C/s) experiment. The mechanisms for such a change in phase transformation kinetics are being further investigated.

CONCLUSION

Neutron diffraction is a unique and powerful tool to study the structures and properties of metallic materials. Recent developments make it possible to apply neutron diffraction in time-resolved study of transient material behavior under fast-changing welding conditions. By utilizing the quasi-steady-state phenomenon and specially designed experimental procedure, the transient temperature and thermal stresses *inside* Al alloy 6061 weld were determined under the complex "real-world" friction-stir welding conditions. The stroboscopic neutron diffraction method, coupled with specimen designed to maintain a uniform temperature in maximum attainable neutron diffraction gage volume, makes it possible to quantify the solid-state phase transformation kinetics of an AHSS under thermal conditions comparable to the welding processes with a subsecond time resolution (~0.1 s). These experimental approaches can be broadly applied to other welding or thermomechanical processes for time-resolved measurement of the fast-changing material state in structural metals.

ACKNOWLEDGEMENT

REFERENCES

1. S.A. David and T. Debroy, *Science* 257, 497 (1992).
2. E.M. Lehockey, G. Palumbo, and P. Lin, *Metall. Mater. Trans. A* 29, 3069 (1998).
3. J.E. Gould, S.P. Khurana, and T. Li, *Weld. J.* 85, 111S (2006).
4. J.A. Francis, W. Mazur, and H.K.D.H. Bhadeshia, *Mater. Sci. Technol.* 22, 1387 (2006).
5. Z. Feng, X.L. Wang, S.A. David, and P.S. Sklad, *Sci. Technol. Weld. Join.* 12, 348 (2007).
6. X. Sun, E.V. Stephens, and M.A. Khaleel, *Eng. Fail. Anal.* 15, 356 (2008).
7. V. Colla, M. Desanctis, A. Dimatteo, G. Lovicu, and R. Valentini, *Metall. Mater. Trans. A* 42A, 2781 (2011).
8. Z. Feng, *U.S. DOE Vehicle Technology Program Annual Report, Characterization of Thermo-Mechanical Behaviors of Advanced High Strength Steels (AHSS): Task 2—Weldability and Performance Evaluations of AHSS Parts for Automotive Structures*, http://www1.eere.energy.gov/vehiclesandfuels/pdfs/alm_06/2z2_feng.pdf (2006).
9. H. Dai, J.A. Francis, H.J. Stone, H. Bhadeshia, and P.J. Withers, *Metall. Mater. Trans. A* 39A, 3070 (2008).
10. A.M. Paradowska, J.W.H. Price, T.R. Finlayson, U. Lienert, and R. Ibrahim, *J. Press. Vessel. Technol. ASME* 132, 011502 (2010).
11. F. Matsuda, H. Nakagawa, K. Shinozaki, Y. Ynishiro, and H. Kihara, *Trans. JWRI* 11, 57 (1982).
12. J.W. Elmer and T.A. Palmer, *Metall. Mater. Trans. A* 37A, 2171 (2006).
13. J.W. Elmer, T.A. Palmer, and E.D. Specht, *Metall. Mater. Trans. A* 38A, 464 (2007).
14. A. Ota, O. Watanabe, K. Matsuoka, Y. Maeda, N. Suzuki, and T. Kubo, *Weld. World* 44, 52 (2000).
15. Z. Yu, W. Zhang, H. Choo, and Z. Feng, *Metall. Mater. Trans. A.* doi:10.1007/s11661 (2011).
16. Y.S. Sato, S.H.C. Park, A. Matsunaga, A. Honda, and H. Kokawa, *J. Mater. Sci.* 40, 637 (2005).
17. W. Woo, H. Choo, M.B. Prime, Z. Feng, and B. Clausen, *Acta Mater.* 56, 1701 (2008).
18. Z. Yu, H. Choo, Z. Feng, and S. Vogel, *Scripta Mater.* 63, 1112 (2010).
19. J. Yang, B.L. Xiao, D. Wang, and Z.Y. Ma, *Mater. Sci. Eng. A-Struct.* 527, 708 (2010).
20. W. Woo, Z. Feng, X.L. Wang, and S.A. David, *Sci. Technol. Weld. Join.* 16, 23 (2011).
21. A.J. Allen, M.T. Hutchings, C.G. Windsor, and C. Andreani, *Adv. Phys.* 34, 445 (1985).
22. X.L. Wang, S. Spooner, C.R. Hubbard, Z. Feng, and B. Taljat, *U.S. DOE Report, Characterization of Welding Residual Stresses with Neutron Diffraction*, http://www.osti.gov/bridge/servlets/purl/672109-1dgma4/webviewable/672109.pdf (1998).
23. T.M. Holden, J.H. Root, D.C. Tennant, and D. Leggett (Paper presented at the 43rd Annual Denver X-Ray Conference on Applications of X-Ray Analysis, vol. 38, 1995, p. 9).

24. W. Reimers, M. Broda, G. Brusch, D. Dantz, K.D. Liss, A. Pyzalla, T. Schmackers, and T. Tschentscher, *J. Nondestruct. Eval.* 17, 129 (1998).
25. J.W.L. Pang, T.M. Holden, and T.E. Mason, *Acta Mater.* 46, 1503 (1998).
26. H. Choo, D. Seo, J. Beddoes, M.A.M. Bourke, and D.W. Brown, *Appl. Phys. Lett.* 85, 4654 (2004).
27. W. Woo, Z.L. Feng, X.L. Wang, K. An, C.R. Hubbard, S.A. David, and H. Choo, *Appl. Phys. Lett.* 88, 261903 (2006).
28. W. Woo, Z. Feng, X.L. Wang, D.W. Brown, B. Clausen, K. An, H. Choo, C.R. Hubbard, and S.A. David, *Sci. Technol. Weld. Join.* 12, 298 (2007). http://www.ingentaconnect.com/content/maney/stwj.
29. H. Choo, P. Rangaswamy, and M.A.M. Bourke, *Scripta Mater.* 42, 175 (1999).
30. X.L. Wang, C.M. Hoffmann, C.H. Hsueh, G. Sarma, C.R. Hubbard, and J.R. Keiser, *Appl. Phys. Lett.* 75, 3294 (1999).
31. R.C. Reed, T. Akbay, Z. Shen, J.M. Robinson, and J.H. Root, *Mater. Sci. Eng. A-Struct.* 256, 152 (1998).
32. E.C. Oliver, T. Mori, M.R. Daymond, and P.J. Withers, *Acta Mater.* 51, 6453 (2003).
33. V.I. Savran, S.E. Offerman, and J. Sietsma, *Metall. Mater. Trans. A* 41A, 583 (2010).
34. T.A. Palmer, J.W. Elmer, P. Mayr, and E.D. Specht, *Sci. Technol. Weld. Join.* 16, 377 (2011).
35. Z. Yu, Z. Feng, K. An, W. Zhang, E.D. Specht, J. Chen, X.L. Wang, and S. David (Paper presented at the Trends in Welding Research 2012: Proceedings of the 9th International Conference, Chicago, IL, 4–8 June 2012).
36. H.R. Wenk, I. Lonardelli, and D. Williams, *Acta Mater.* 52, 1899 (2004).
37. D.W. Brown, S.R. Agnew, M.A.M. Bourke, T.M. Holden, S.C. Vogel, and C.N. Tome, *Mater. Sci. Eng. A-Struct.* 399, 1 (2005).
38. P.J. Withers, *J. Appl. Crystallogr.* 37, 607 (2004).
39. C.G. Windsor, *Pulsed Neutron Scattering*, 1st ed. (London, U.K.: Taylor and Francis, 1981).
40. P.J. Withers, *C.R. Phys.* 8, 806 (2007).
41. J. Wong, T. Ressler, and J.W. Elmer, *J. Synchrotron Radiat.* 10, 154 (2003).
42. W. Woo, Z. Feng, X.L. Wang, K. An, W.B. Bailey, S.A. David, C.R. Hubbard, and H. Choo, *Residual Stresses Vii* 524–525, 387 (2006).
43. C.J. Dawes and W.M. Thomas, *Weld. J.* 75, 41 (1996).
44. N. Sreenivasan, M. Xia, S. Lawson, and Y. Zhou, *J. Eng. Mater. Technol. ASME* 130, 041004 (2008).
45. M.I. Khan, M.L. Kuntz, and Y. Zhou, *Sci. Technol. Weld. Join.* 13, 294 (2008).
46. X.L. Wang, T.M. Holden, G.Q. Rennich, A.D. Stoica, P.K. Liaw, H. Choo, and C.R. Hubbard, *Phys. B-Condensed Matter* 385, 673 (2006).
47. R.B. Vondreele, J.D. Jorgensen, and C.G. Windsor, *J. Appl. Crystallogr.* 15, 581 (1982).
48. R.J. Hill and C.J. Howard, *J. Appl. Crystallogr.* 20, 467 (1987).
49. X.L. Wang, J.A. Fernandezbaca, C.R. Hubbard, K.B. Alexander, and P.F. Becher, *Phys. B* 213, 824 (1995).
50. A.C. Larson and R.B. Von Dreele, *General Structure Analysis System (GSAS)*. http://www.ccp14.ac.uk/ccp/ccp14/ftp-mirror/gsas/public/gsas/manual/GSASManual.pdf (2000).
51. B.H. Toby, *J. Appl. Crystallogr.* 34, 210 (2001).
52. M.R. Daymond and P.J. Withers, *Scripta Mater.* 35, 717 (1996).
53. T.C. Hansen, *Eur. Powder Diffr. EPDIC* 8, 181 (2004).
54. N. Jia, Z.H. Cong, X. Sun, S. Cheng, Z.H. Nie, Y. Ren, P.K. Liaw, and Y.D. Wang, *Acta Mater.* 57, 3965 (2009).